

# CHARACTERIZATION OF THE BNL ATF COMPTON X-RAY SOURCE USING K-EDGE ABSORBING FOILS\*

O. Williams, G. Andonian, E. Hemsing, J. Rosenzweig

UCLA Department of Physics, Los Angeles, CA 90095, U.S.A.

M. Babzien, K. Kusche, J. Park, I. Pogorelsky, V. Yakimenko, BNL ATF, Upton, NY 11973, U.S.A.

## Abstract

Spectral and angular information of inverse Compton sources is shown to be obtainable using only an x-ray imaging device and various foils with K-edges in the many keV energy range. Beam parameters can be chosen such that on-axis photons are above the K-edge for a given material, where absorption is very strong and there is relatively zero transmission. Photons observed off-axis are red-shifted and fall below the K-edge, therefore being transmitted and creating an on-axis null. The electron beam energy necessary to create the null is an indicator of the bandwidth. We present experimental results of the bandwidth and double differential spectrum (DDS) for angle and energy of Compton photons generated at the BNL ATF.

## INTRODUCTION

The production of high peak brightness ( $\geq 10^{19}$  photons/s/mm<sup>2</sup>/mrad<sup>2</sup> in 0.1% bandwidth) radiation by the interaction of a relativistic electron beam with a high power laser pulse provides for unique research opportunities in medicine, anthropology, materials and ultra-fast science requiring short wavelengths.

In Compton scattering, there is a transfer of energy between electron and photon, where the electron is generally taken to be at rest and the photon loses energy. For inverse Compton scattering (ICS), the electron is relativistic and imparts a large energy gain on the scattered photon. The basic expression for the scattered photon energy as a function of beam parameters can be written as,

$$E_x = \frac{2\gamma^2(1 - \cos \Phi)}{\left(1 + \frac{a_L^2}{2} + \gamma^2\theta^2\right)} E_L \quad (1)$$

where  $\gamma$  is the relativistic Lorentz correction factor of the e-beam,  $\Phi$  is the laser interaction angle ( $\pi$  for head-on collision),  $\theta$  is the source observation half-angle,  $E_L$  is the laser photon energy and  $a_L$  is the normalized laser vector potential.  $a_L$  can be expressed conveniently as [1],

$$a_L = 0.85 \times 10^{-9} \lambda_L [\mu\text{m}] \sqrt{I_0 [\text{W}/\text{cm}^2]} \quad (2)$$

where  $\lambda_L$  is the laser wavelength and  $I_0$  is the laser intensity.

Electron beams with picosecond bunch lengths interacting at 180° with lasers produce picosecond x-ray pulses. These scattered photons are polarized in the

direction of the incident laser polarization and have an energy-angle correlation and small bandwidth, allowing for monochromatization via apertures. The bandwidth is dependent on various beam parameters and interaction geometry and requires optimization as demanded by user applications.

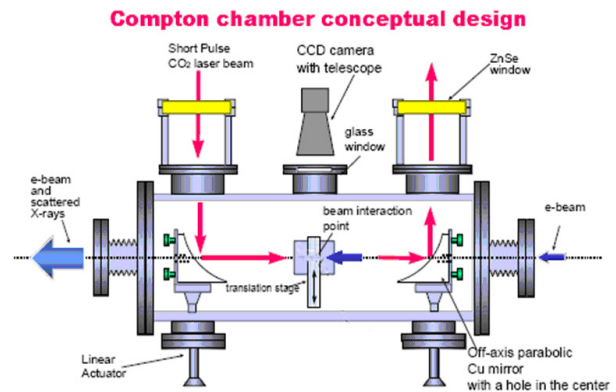


Figure 1: ICS interaction chamber [2].

## SOURCE DESIGN

The layout of the source is shown above in Figure 1 and discussed elsewhere [2, 3]. The two beams are aligned spatially by maximizing transmission through a 150  $\mu\text{m}$  pinhole at the IP and then rastering the e-beam until the x-ray signal is maximized. Synchronization is done using a germanium crystal. When the high charge density electron beam hits the crystal, a semiconductor plasma is formed, which reflects the 10  $\mu\text{m}$  laser pulse [4]. This provides for picosecond timing resolution between the

Table 1: Beam Parameters

Electron Beam	Value	Laser Beam	Value
Energy	66 MeV	Pulse energy	2 J
Beam size (RMS)	30 $\mu\text{m}$	Laser wavelength	10.6 $\mu\text{m}$ (0.117 eV)
Emittance (RMS)	2 $\mu\text{m}$	Waist size (RMS)	60 $\mu\text{m}$
Energy spread	0.5% (1.0%)	Pulse length (FWHM)	6 ps
Charge	300 pC	Simulated laser potential	0.38
Bunch length (FWHM)	4 ps (300 fs)	Laser bandwidth	~0.6%

two beams [5]. Electrons are dumped by a dipole magnet where energy spread and charge can be measured. Beam parameters for the 180° interaction and resultant simulated source parameters are shown in Table 1.

### X-RAY DIAGNOSTICS

Because the source bandwidth is expected to be <5%, it is necessary to have an energy diagnostic of good resolution. The absorption K-edge of an element is very energy dependent, absorbing photons strongly at and above the K-edge energy. Using this knowledge, one can make a foil of certain thickness and material with K-edge near that of the scattered photon energy, which greatly attenuates photons above the K-edge and transmits others. This low pass filter, essentially, can be used with a flux diagnostic and imaging device to see the energy-angle correlation and bandwidth of the source.

From Table 2, the x-ray energy is ~ 7 keV, so we must select an element with K-edge close to this and which can be easily made into a thin foil. Iron and Nickel are fairly simple foils to make and have K-edges at 7.112 keV and 8.33 keV, respectively. Transmission curves for 50 μm Fe and Ni foils and a 20 μm Ag foil (with no absorption edge in range) are plotted in Figure 2 [6].

Table 2: Source Parameters

Scattered Photon	Value
Total flux	$1 \times 10^9$ ( $2 \times 10^7$ ) photons
Photon energy	7.85 keV
Pulse length	0.3-4 ps
Bandwidth	2-3%
Source size	22 μm
Acceptance angle	8 mrad (1 mrad)
Peak brightness	$B_{\text{peak}} = 3.6 \times 10^{20}$

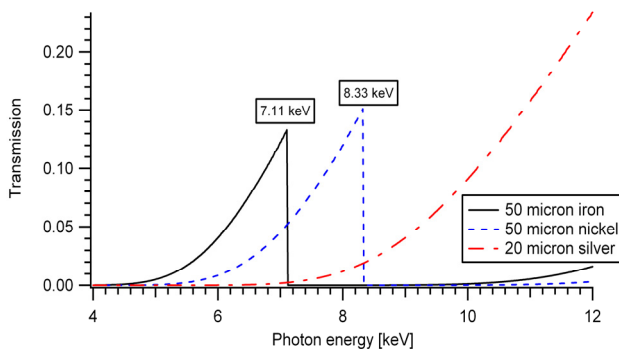


Figure 2: Foil transmission curves.

A Si-diode is used to measure the x-ray flux, while a microchannel plate (MCP) image intensifier [7] (~2% QE, variable  $10^7$  gain), with a TE-cooled CCD camera is used for imaging. The spectral response for both detectors is nearly linear in our energy range.

### Light Sources and FELs

#### T15 - Undulators and Wigglers

It can be seen from (1) that photons are red-shifted when observed off axis by an angle  $\theta$ . This means on axis photons just above the foil K-edge will be attenuated, while off axis photons will lie just below and transmit. This should produce a null with surrounding high intensity regions of 7.1 keV photons. The distance between regions should shrink in size for lower e-beam energy,  $\gamma$ , or for any red-shifting effects, e.g. nonlinear scattering ( $a_L > 0.1$ ) or angles in the electron beam. It should be noted, however, that for large bandwidth the null will tend to close as the energy-angle correlation is lost due to the smeared spectrum, complicating image analysis. Plotted in Figure 3 is a simulation [8] of the expected transverse image of the x-rays.

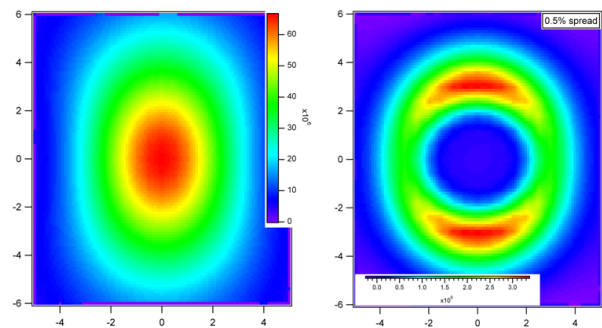


Figure 3: Simulated angular distribution of source before (left) and after (right) passing through 50 μm iron foil.

Iron, nickel, and silver foils were placed on remote flippers in air and aligned with the x-ray vector. The Si-diode detector was placed on a remotely insertable stage, followed by another 250 μm beryllium window and the MCP intensifier. A pinhole on a 2-axis assembly allows for angle selection and subsequent flux measurement.

In order to verify the effect of the foils on the x-rays, we started with an electron beam energy of 72 MeV, assuring that we were well above the K-edge for both Fe (7.11 keV) and Ni (8.33 keV), including red-shifted photons off axis. Below are x-ray images taken after passing through the foils.

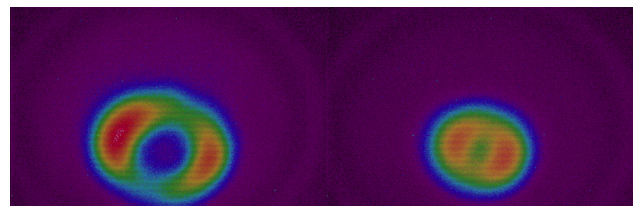


Figure 4: Source profile after passing through iron (left) and nickel foils.

A clear difference in hole size is seen between Fe and Ni foils due to the nickel K-edge being 1.2 keV above that of iron, causing fewer on axis photons to be above and thus absorbed. The Ag foil preferentially attenuates lower energy, off axis photons, as expected.

A scan of the electron beam energy was made from 64-72 MeV and corresponding x-ray images were taken (examples, below). The expected increase in lobe

separation due to the foil K-edge for increasingly higher e-beam energy is clear and reveals the off axis red-shift. Assuming the photon energy at a lobe is peaked at 7.1 keV, and plotting the expected (eqn. 1) and observed angle, we see fairly good agreement (see Figure 6).

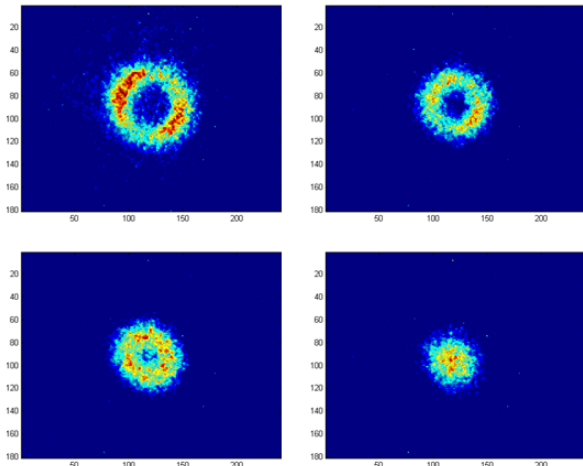


Figure 5: X-ray images after passing through Fe foil for 68, 66 (top), 65, and 64 (bottom) MeV electron beams.

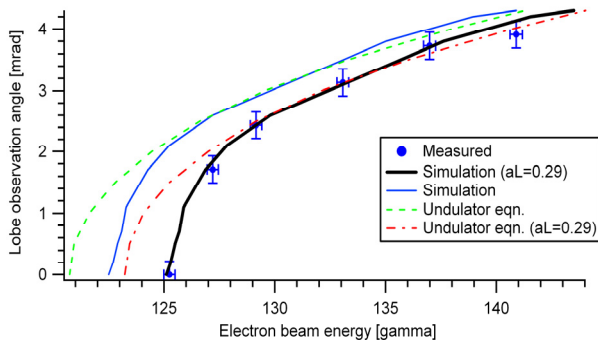


Figure 6: Lobe observation angle and corresponding e-beam energy. Simulation was red-shifted by an appropriate amount ( $\sim 290$  eV) to fit measured data and corresponds to  $a_L=0.29$ .

The laser polarization was switched to circular in subsequent runs and the x-ray count for a compressed, 300 fs electron beam measured. Shown in Figure 7, the source asymmetry is gone due to electron motion in both transverse directions. A clear increase in bandwidth (and red-shifting) can be observed for the compressed beam due to higher energy spread and larger beam angles, but results in an x-ray pulse length of 300 fs.

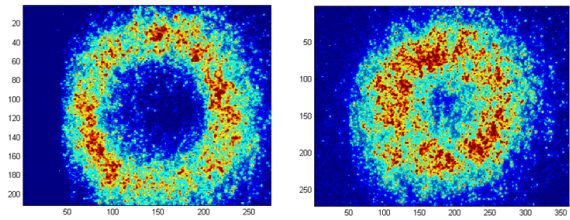


Figure 7: Images of x-rays from a circularly polarized laser, 68 MeV electron beam, uncompressed (left,  $\sim 4$  ps) and compressed (right,  $\sim 300$  fs) passing through Fe foil.

A bandwidth is extracted from figure 4 by looking at the null size ( $\sim 1$  mrad) made when going from 64 MeV to 66 MeV. This corresponds to an increase of photon energy by about 5%. If a negligible number of photons leak through the null, then the lower energy photons from bandwidth are being compensated for by the increase in beam energy and absorbed in the foil. This persuades us to say that the bandwidth is roughly  $< 5\%$ . When the 1 mrad pinhole is placed on axis and the foil removed,  $2 \times 10^6$  photons are detected on the Si-diode detector after considering attenuation in air and the Be-window.

## CONCLUSIONS

Characterization of the ICS source at the BNL ATF has been done using thin foils with K-edges near the source photon energy. Off-axis red-shifting as predicted by (1) has been observed and there is a clear difference between linear and circular polarizations.  $10^6$  photons within 5% bandwidth have been measured over 1 mrad on axis, resulting in a measured peak brightness of  $2.4 \times 10^{19}$  photons/mm<sup>2</sup>/mrad<sup>2</sup>/s/0.1% BW.

## REFERENCES

- [1] E. Esarey, et al, Phys. Rev. E 48, 3003 (1993).
- [2] I. V. Pogorelsky, et al, Phys. Rev. STAB 3, 090702 (2000).
- [3] M. Babzien, et al, Phys. Rev. Letters 96, 054802 (2006).
- [4] P. B. Corkum, et al, J. Appl. Phys. 50 (5) 3079 (May 1979).
- [5] S. Tochitsky, et al, Physics of Plasmas 11, No. 5, 2875 (2004).
- [6] Center for X-ray Optics, X-ray Tools; [http://henke.lbl.gov/optical\\_constants/filter2.html](http://henke.lbl.gov/optical_constants/filter2.html).
- [7] Burle Electro-optics, microchannel plate detectors; <http://www.burle.com/>
- [8] W. J. Brown, et al, Phys. Rev. STAB 7, 060703 (2004).